

Pyroxenites and Chromite Mineralization of the Sangalyk Sector, Southern Urals

D. N. Salikhov^a, G. I. Belikova^a,
Corresponding Member of the RAS V. N. Puchkov^a, and T. N. Moroz^b

Received December 19, 2006

DOI: 10.1134/S1028334X07050285

The nature of chromite ores is controversial. Previously, they were considered as products of the layering of ultramafic magma [2–4, 6]. A new hypothesis based on the genetic relation between chromites and secondary dunites has been proposed in recent works [5, 8, 10]. The formation of secondary dunites is related to the partial melting of peridotites (more precisely, the pyroxene component of peridotites) [1], resulting in the separation of primarily restitic dunites, an ore-bearing chromite portion, and a melt with a basalt (gabbro) composition. Thus, secondary dunites have a genetic relation with gabbro.

Chromite mineralization is also recorded in autonomous intrusion phases (lenses among ultramafic bodies and dikes) composed of pyroxenites. The present paper discusses a case history of such bodies.

The Sangalyk area (Uchaly ore district, southern Urals) incorporates small outcrops of disseminated chromite ores associated with pegmatoid pyroxenites (Fig. 1). We studied a small lens with an apparent thickness of 40–45 cm and unknown length. The lens shows a distinct zoning (Fig. 2). The endocontact zone with massive chromite ore is divided into two (ore and near-ore) subzones. The near-ore subzone is mainly composed of fine-grained chrome diopside with stringers and dissemination of chromite and alumochromite. The transitional zone between the ore zone and the central pyroxenite zone consists of large (up to 8 cm) twinned zonal pyroxene crystals.

We investigated the mineral composition of the lens by various physical and physicochemical methods. The atomic absorption, spectrophotometric, and optical microscopic analyses were carried out at the Institute of Geology (Ural Scientific Center, Russian Academy of

Sciences). IR-spectroscopy, scanning by electron microscope equipped with an energy-dispersive spectrometer (SEM-EDS analysis), and electron microprobe analysis were performed at the Institute of Geol-

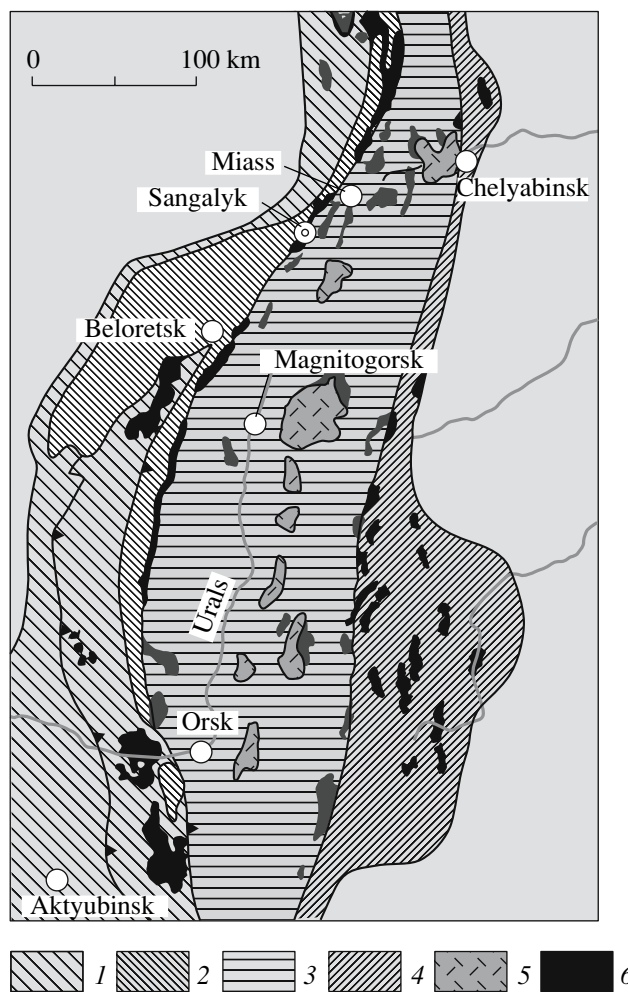


Fig. 1. Location of the Sangalyk Highland in the Uralian structure. (1) West Ural zone; (2) Uraltau zone; (3) Tagil–Magnitogorsk zone; (4) East Ural zone; (5) granite massifs; (6) ultramafic massifs.

^a Institute of Geology, Ufa Scientific Center, Russian Academy of Sciences, ul. Karla Marksa 16/2, Tsent, Ufa, 450000 Russia; e-mail: magm@anrb.ru

^b Institute of Geology and Mineralogy, Siberian Division, Russian Academy of Sciences, pr. akademika Koptyuga 3, Novosibirsk, 630090 Russia

ogy and Mineralogy (Siberian Division, Russian Academy of Sciences). The XRD analysis was carried out at the Institute of Geology and Mineralogy (Siberian Division, Russian Academy of Sciences) and the Institute of Problems of Metal Superplasticity, Russian Academy of Science. The mode of the investigation of separate sectors of the lens was governed by the degree of complexity of their mineral compositions.

The averaged chemical compositions of the near-ore subzone, transitional zone, and central part of the lens demonstrate a distinct microzonality (Table 1). The lens is characterized by the following specific chemical features (Table 2): (1) the rocks correspond to Ca- and Al₂O₃-rich pyroxenites with Ca dominating over Mg (in some places, Ca ≥ Mg); (2) when passing from the transitional zone to the central zone, the rocks are depleted in Fe# and Cr#, but enriched in Mg# and Al#. These facts imply variation of the mineral composition in different zones, in particular, increase in the share of Ca- and Mg-bearing silicate minerals toward the central zone.

Investigation of microzones with various methods revealed that the pyroxenite zone has a complex and heterogeneous mineral composition. Chromite, alumochromite, and magnetite are the major minerals in thin sections of the ore (endocontact) zone. The near-ore subzone has a more diverse mineral composition. The coarse-dispersed mass includes separate well-developed crystallites and aggregates (~0.1–2.5 mm) of chrome spinels or their intergrowths with pyroxene crystals. The chrome spinel crystallites are often enclosed as solid phase inclusions in pyroxene grains. This is distinctly observed in the transparent emerald-green diopside grains.

The results of IR-spectroscopic analysis showed that mineral grains from the near-ore subzone have a complex and heterogeneous phase composition. Microlitic intergrowths represent the Fe-chlorite–hedenbergite or diopside–chromite–Fe-chlorite association (in some cases, the hedenbergite–diopside association). The XSA revealed that the intergrowths are composed of crystallites of Mg–Fe-silicates (hedenbergite, diopside, Cr-diopside, and rare wollastonite) and chrome spinels (alumochromite and chromite). Chlorites (Cr-amesite and Fe-chlorite) are also present.

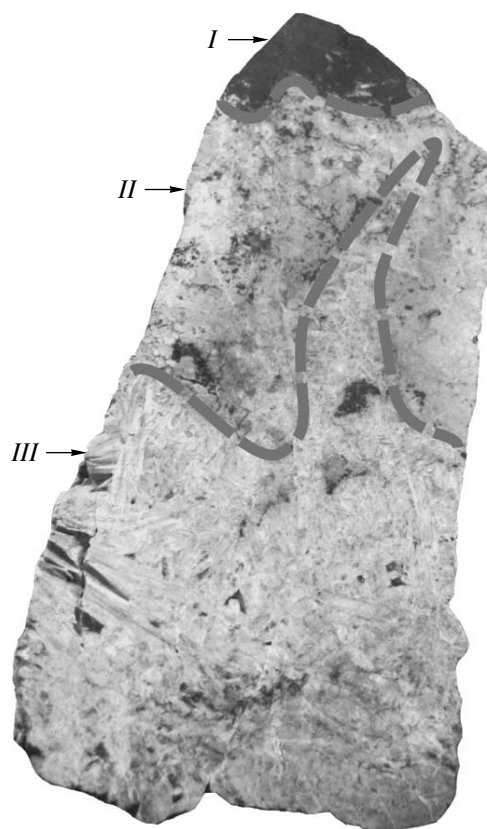


Fig. 2. Zonality of the chromite-bearing pyroxenite body. Zones: (I) ore, (II) transitional, (III) central.

IR spectra of pyroxenes from the diopside–hedenbergite series show a shift of Mg–O bands toward lower frequencies, suggesting isomorphous transitions, e.g., Fe²⁺ → Mg²⁺.

The heterogeneity and complexity of the mineral composition of the near-ore subzone are also confirmed by electron microprobe data on various sections of grains. We recorded distinct differentiation in the distribution of Cr, Mg, and Ca contents in different fragments of the mineral matrix. The microprobe data indicate that the distinct macrozonality of the lens reflects microheterogeneity of the mineral composition related to genetic features.

Table 1. Averaged composition of the pyroxenite lense in different zones, wt %

Part of the lens	SiO ₂	TiO ₂	Al ₂ O ₃	Cr ₂ O ₃	FeO	Fe ₂ O ₃	MnO	MgO	CaO	Na ₂ O	K ₂ O	P ₂ O ₅	L.O.I	Total
I	n.d.	n.d.	20.65	22.50	21.00	n.d.	n.d.	9.00	n.d.	n.d.	n.d.	n.d.	n.d.	
II	45.15	0.120	5.72	0.624	4.25	n.d.	0.037	11.03	29.53	0.37	0.006	0.095	n.d.	96.93
	49.31	0.01	4.93	1.410	2.24	2.30	0.07	16.76	22.40	0.10	0.02	0.09	0.45	100.09
III	53.00	0.01	1.80	0.067	1.44	0.76	0.05	18.00	23.42	0.50	0.02	0.01	0.60	99.68

Note: Here and in Table 2: (I) near-ore subzone at the exocontact of the lens; (II) near-ore/pyroxenite transitional zone; (III) central zone. (n.d.) Not determined.

Table 2. Calculated parameters of chemical compositions of different parts of the lens

Part of the lens	Fe [#] , %	Al [#] , %	Cr [#] , %	Mg [#] , %	Ca : Mg
I		41.50	58.30		
II	33.16	87.64	12.36	66.83	3.17
	14.69	73.09	26.98	85.32	1.58
III	9.47	95.36	4.01	90.65	1.54

Note: $Fe^{\#} = 100 \cdot Fe/(Fe + Mg)$, $Al^{\#} = 100 \cdot Al/(Al + Cr)$, $Cr^{\#} = 100 \cdot Cr/(Cr + Fe)$, $Mg^{\#} = 100 \cdot Mg/(Mg + Fe)$.

The SEM-EDS analysis made it possible to determine the mineral composition at separate points of grains in the near-ore subzone and transitional zone. Based on the XSA data, large crystals in the central zone include alternation of laminae of diopside and wollastonite with minor traces of enstatite and hypersthene. Intergrowth of cognate minerals promoted the microzonal structure of crystals manifested as alternation of differently colored bands.

Diopside and wollastonite differ in structure. However, they have several similar crystallographic properties that fostered their crystallization from melts with the formation of solid solutions. This process was also promoted by the similarity of adjusted values of melting entropy (Fig. 3). Owing to structural distinctions, cooling of the pyroxene solid solution is accompanied by the crystallization of autonomous phases of diopside, wollastonite, and admixtures.

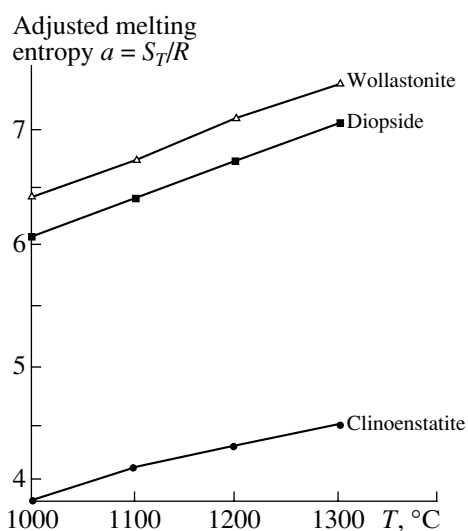


Fig. 3. Temperature dependence of entropy values of wollastonite, diopside, and clinoenstatite. S values [9] were used in calculations.

Thermodynamic calculations of constraints of wollastonite crystallization [7] showed that the incongruent melting of wollastonite in the Hd–Wol_{ss} system is terminated at a pressure of ~13 kbar and temperature of ~1270°C. The stability field of wollastonite depends to a great extent on pressure and is constrained by $T = 1150–1270^{\circ}\text{C}$ and $P \sim 5–13$ kbar. The formation conditions of pyroxenes from the central zone of the lens are probably similar to the parameters of wollastonite stability indicated above.

Comprehensive investigation of chromite ore and the associated pyroxenes showed that the ore lens is a product of sequential crystallization from the endocontact zone to the inner part of the lens. Chrome spinels were crystallized from the metalliferous secondary melt produced by the fusion of spinel peridotite pyroxenes. The chromite ore is consolidated in the endocontact zone of the pyroxenite lens.

ACKNOWLEDGMENTS

This work was supported by the Division of Earth Sciences of the Russian Academy of Sciences (fundamental research program no.4).

REFERENCES

1. S. G. Kovalev and D. N. Salikhov, *Mineral Resources of Bashkortostan: Chromite Ores* (Ekologiya, Ufa, 2000) [in Russian].
2. R. G. Coleman, *Ophiolites* (Springer, Berlin, 1976; Mir, Moscow, 1979).
3. A. A. Marakushev, *Petrogenesis and Ore Formation* (Nauka, Moscow, 1979) [in Russian].
4. N. V. Pavlov, G. G. Kravchenko, and I. I. Chuprynina, *Chromites of the Kempirsai Pluton* (Nauka, Moscow, 1968) [in Russian].
5. E. V. Pushkarev, *The Uktus Dunite–Clinopyroxenite–Gabbro Massif: Information Materials* (Ural. Otd. Ross. Akad. Nauk, Yekaterinburg, 1999) [in Russian].
6. G. A. Sokolov, *Uralian Chromites, Their Compositions, Crystallization Conditions, and Distribution Patterns* (Akad. Nauk SSSR, Moscow, 1948) [in Russian].
7. D. H. Lindsley, in *Experimental Petrology and Mineralogy* (Nedra, Moscow, 1971) [in Russian].
8. F. Melcher, W. Grum, T. V. Thalhammer, and O. A. R. Thalhammer, *Miner. Deposita* **34**, 250 (1999).
9. R. A. Robie and B. S. Hemingway, *Thermodynamic Properties of Minerals and Related Substances at 298.15 K and 1 Bar (10⁵ Pascal's) Pressure and at Higher Temperatures* (US Govt. Print. Off., 1978).
10. F. Zaccarini, E. V. Pushkarev, G. B. Fershtater, and G. Garuti, *Can. Miner.* **42**, 545 (2004).